Available online at www.sciencedirect.com
ScienceDirect
Trans. Nonferrous Met. Soc. China 26(2016) 2485−2494
Transactions of Nonferrous Metals Society of China
www.tnmsc.cn

Formation and evolution of secondary minerals during bioleaching of chalcopyrite by thermoacidophilic Archaea *Acidianus manzaensis*

Hong-chang LIU [1,2], Jin-lan XIA [1,2], Zhen-yuan NIE[1,2], Wen WEN[3], Yun YANG[1,2], Chen-yan MA[4], Lei ZHENG[4], Yi-dong ZHAO[4]

1. School of Minerals Processing and Bioengineering, Central South University, Changsha 410083, China;
2. Key Lab of Biometallurgy Ministry of Education, Central South University, Changsha 410083, China;
3. Shanghai Synchrotron Radiation Facility, Shanghai Institute of Applied Physics, Chinese Academy of Sciences, Shanghai 201204, China;
4. Beijing Synchrotron Radiation Facility, Institute of High Energy Physics, Chinese Academy of Sciences, Beijing 100049, China

Received 25 March 2015; accepted 28 June 2016

Abstract: The formation and evolution of secondary minerals during bioleaching of chalcopyrite by thermoacidophilic Archaea *Acidianus manzaensis* were analyzed by combining synchrotron radiation X-ray diffraction (SR-XRD) and S, Fe and Cu K_α X-ray absorption near edge structure (XANES) spectroscopy. Leaching experiment showed that 82.4% of Cu^{2+} was dissolved by *A. manzaensis* after 10 d. The surface of chalcopyrite was corroded apparently and covered with leaching products. During bioleaching, the formation and evolution of secondary minerals were as follows: 1) little elemental sulfur, jarosite, bornite and chalcocite were found at days 2 and 4; and 2) bornite and chalcocite disappeared, covellite formed, and jarosite gradually became the main component at days 6 and 10. These results indicated that metal-deficiency sulfides chalcocite and bornite were first formed with a low redox potential value (360−461 mV), and then gradually transformed to covellite with a high redox potential value (461−531 mV).

Key words: bioleaching; chalcopyrite; *Acidianus manzaensis*; secondary minerals; formation; evolution

1 Introduction

Biohydrometallurgy is an emerging technology and takes an important role in copper recovery from low grade metal sulfides with attractively economic, environmental and social benefits [1]. Among these metal sulfides, chalcopyrite is the most abundant and widespread. However, it is the most refractory and recalcitrant to both chemical and biological leaching because of the forming of surface layer and iron deficient secondary minerals [2,3].

During the dissolution of chalcopyrite, the release of iron into electrolyte was usually faster than copper, and the iron deficient secondary minerals covellite, chalcocite, and metastable layers ($Cu_{1-x}S$ or $Cu_{1-x}Fe_{1-y}S_2$) were assumed [4−7]. However, the consistent evidence about metal-deficient sulfides was rarely reported. One difficulty for studying the surface chemicals of chalcopyrite during bioleaching is that some of the metal-deficient secondary minerals are less abundant and could be unstable transition states [2]. This problem could be resolved with emerging of the third generation synchrotron radiation (SR) [8], which is an ideal X-ray source with high spatial resolution and high sensitivity for probing trace metallic elements [9].

In our previous studies, SR-based X-ray absorption near edge structure (XANES) spectroscopy was used to study the surface sulfur speciation during bioleaching of chalcopyrite [10−12]. However, some important

Foundation item: Project (U1232103) supported by the Joint Funds of National Natural Science Foundation of China and Large Scientific Facility Foundation of Chinese Academy of Sciences; Project (51274257) supported by the National Natural Science Foundation of China; Project (CX2014B092) supported by Hunan Provincial Innovation Foundation For Postgraduate, China; Project (VR-12419) supported by Beijing Synchrotron Radiation Facility Public User Program, China; Projects (13SRBL15U13024, 13SRBL14B13023) supported by the Open Funds of Shanghai Synchrotron Radiation Facility, China

Corresponding author: Jin-lan XIA; Tel: +86-731-88836944; E-mail: jlxia@csu.edu.cn

DOI: 10.1016/S1003-6326(16)64369-8

information in the dissolution process could be missed merely based on sulfur speciation, because the role of copper and iron speciation also makes contribution to the leaching process. In order to learn the concrete details of the dissolution mechanism, the comprehensive analyses based on Cu, Fe and S speciation transformation should be combined. The SR-based X-ray diffraction (SR-XRD) has an advantage over conventional XRD because of higher signal/noise ratio and spatial resolution and it can be of value for analyzing the structures and composition of compounds on surface of minerals [13]. Therefore, by combining SR-XRD and XANES, the surface chemical species can be qualitatively and quantitatively analyzed, which could provide more convincing results and be useful for understanding the dissolution mechanism of chalcopyrite.

On the other hand, bioleaching of chalcopyrite with extremely thermoacidophilic microorganisms has become a focus recently, because they could grow at high temperature (>60 °C), accelerate the reaction rate and dissolve the highly refractory ores, thus leading to higher metal recovery compared with mesophiles and moderate thermophiles [1,14]. Therefore, in the present study, the formation and evolution of secondary minerals during bioleaching of chalcopyrite by typically thermoacidophilic Archaea *Acidianus manzaensis* were analyzed by combining SR-XRD and S, Fe and Cu K_α XANES spectroscopy. It could be useful for better understanding the dissolution mechanism of chalcopyrite during bioleaching.

2 Experimental

2.1 Strain and culture medium

The thermoacidophilic Archaea strain *A. manzaensis* YN-25 (accession number of 16S rDNA in GeneBank: EF522787) was provided by the Key Laboratory of Biometallurgy of Ministry of Education of China, Changsha, China. The basal medium for *A. manzaensis* cultivation consisted of the following components: 3.0 g/L $(NH_4)_2SO_4$, 0.5 g/L $MgSO_4{\cdot}7H_2O$, 0.5 g/L K_2HPO_4, 0.1 g/L KCl, 0.01 g/L $Ca(NO_3)_2$, and 0.2 g/L yeast extracts.

2.2 Mineral samples

The standard chalcopyrite ($CuFeS_2$), covellite (CuS), chalcocite (Cu_2S) and jarosite ($KFe_3(SO_4)_2(OH)_6$) samples used in this study were provided by School of Minerals Processing and Bioengineering, Central South University, Changsha, China. The mineralogical compositions tests (by XRD) indicated that the original chalcopyrite minerals are mainly chalcopyrite. X-ray fluorescence spectroscopic analysis showed that the content of the original chalcopyrite contained (mass fraction, %): Cu, 32.6; S, 31.05; Fe, 27.11; O, 2.7; Zn, 1.94; Ba, 0.50; Ca, 0.43; Si, 0.37; Al, 0.17; Mg, 0.09. The mineral was ground to fine powder, which was passed through a sieve of 75 μm but was retained by a sieve of 38 μm, guaranteeing the particle size was 37−75 μm.

2.3 Bioleaching experiment

Before the bioleaching experiments, the strain was initially activated and pretreated according to LIANG et al [15]. Then *A. manzaensis* was incubated in 500 mL Erlenmeyer flasks containing 200 mL sterilized basal medium and 2 g chalcopyrite in a high-temperature bath rotary shaker (SHZ-GW) at 65 °C and 170 r/min. The initial pH of the culture medium was firstly adjusted to 1.85 with dilute sulfuric acid. The initial inoculated cell density was 2×10^7 cells/mL. The abiotic control groups (without *A. manzaensis*) were carried out with the same culture medium. All above experiments were performed in triplicate at the same conditions for 10 d. Evaporated water was compensated with sterilized ultra-pure water based on mass loss at twelve-hour intervals.

2.4 Analysis methods

During leaching of chalcopyrite by *A. manzaensis*, sample solutions were taken out at 2 d intervals to monitor cell densities, pH and redox potential values, $[Fe^{2+}]$, $[Fe^{3+}]$ and $[Cu^{2+}]$ according to the previous descriptions [16,17]. The surface morphology of chalcopyrite residues during leaching experiment was observed by scanning electron microscopy (SEM) (Nova™ NanoSEM 230, FEI, USA) according to previous description [18].

In order to investigate the formation and evolution of secondary minerals on mineral surfaces, both the original mineral samples and leaching residues at different leaching time were characterized by SR-XRD and S, Fe, Cu K-edge XANES spectroscopy, respectively. The SR-XRD analysis was recorded at beamline BL14B1 of Shanghai Synchrotron Radiation Facility (SSRF), Shanghai, China, at a step of 0.01 ° and a dwell time of 0.5 s at each point. The S, Fe, Cu K-edge XANES spectra were recorded according to previous descriptions [17,19]. Then, the XANES spectra were normalized and fitted for their linear combinations using the standard spectra with IFEFFIT program [20].

3 Results and discussion

3.1 Leaching parameters of chalcopyrite by *A. manzaensis*

The leaching parameters of chalcopyrite by *A. manzaensis* and in sterile control experiment were characterized in terms of the cell density, pH and redox

potential values, and copper and iron ions concentrations (Figs. 1(a) and (d)), respectively. Results in Fig. 1(a) showed that the cell density in the bioleaching solution reached a maximum of 3.07×10^8 cell/mL at day 6, and then decreased. After 10 d, the Cu^{2+} concentration was 2.72 g/L, corresponding to 82.4% copper extraction, compared with that of 0.36 g/L in sterile control experiment (Fig. 1(c)), indicating that the thermoacidophilic Archaea *A. manzaensis* could significantly promote copper extraction, which was in accordance with the results of LIANG et al [21] and GERICKE et al [22].

During bioleaching, the pH value decreased with the increase of time, and decreased rapidly at days 2−6 (Fig. 1(a)). The redox potential value increased with time and tended to slow when reached 531−550 mV, which showed similar trend as Cu^{2+} concentration (Fig. 1(a)). By contrast, results in Fig. 1(c) showed that, in the sterile control experiment, pH values were slowly increased with the increase of time. Redox potential values were gradually increased at day 0−6 from 308 to 328 mV and then basically unchanged.

It can be seen from Fig. 1(b) that the concentrations of total iron ions and Fe^{3+} apparently increased and reached the maximum values at day 4, and then dropped apparently at day 6 and finally remained unchanged. The Fe^{2+} concentration reached the maximum value at day 2, and gradually dropped to approach zero, which probably was caused by the growth of *A. manzaensis*. Results in Fig. 1(d) showed that in sterile control experiment the total iron ions concentration was fast increased initially and then changed little. Meanwhile, the Fe^{3+} concentration was basically zero.

The dissolution of chalcopyrite is very complex, which could be attacked by Fe^{3+} or proton in acid solutions, generally presented as Eqs. (1)−(2) [1,23], in which ferric ions or oxygen are the oxidant and the sulfide components of chalcopyrite are oxidized to elemental sulfur. Then the intermediate, e.g., elemental sulfur and ferrous ions, can be oxidized by sulfur oxidizing microorganism and iron oxidizing microorganism and regenerate the proton and Fe^{3+} consumed at the beginning Eqs. (3) and (4) [24].

$$CuFeS_2+4Fe^{3+}\xrightarrow{\text{Chemical}}Cu^{2+}+2S^0+5Fe^{2+} \quad (1)$$

$$CuFeS_2+4H^++O_2\xrightarrow{\text{Chemical}}Cu^{2+}+2S^0+Fe^{2+}+2H_2O \quad (2)$$

$$2S^0+2H_2O+3O_2\xrightarrow{\text{Sulfur oxidizing microbial}}2SO_4^{2-}+4H^+ \quad (3)$$

$$4Fe^{2+}+4H^++O_2\xrightarrow{\text{Chemical/Iron oxidizing microbial}}4Fe^{3+}+2H_2O \quad (4)$$

Copper extraction from chalcopyrite is an acid

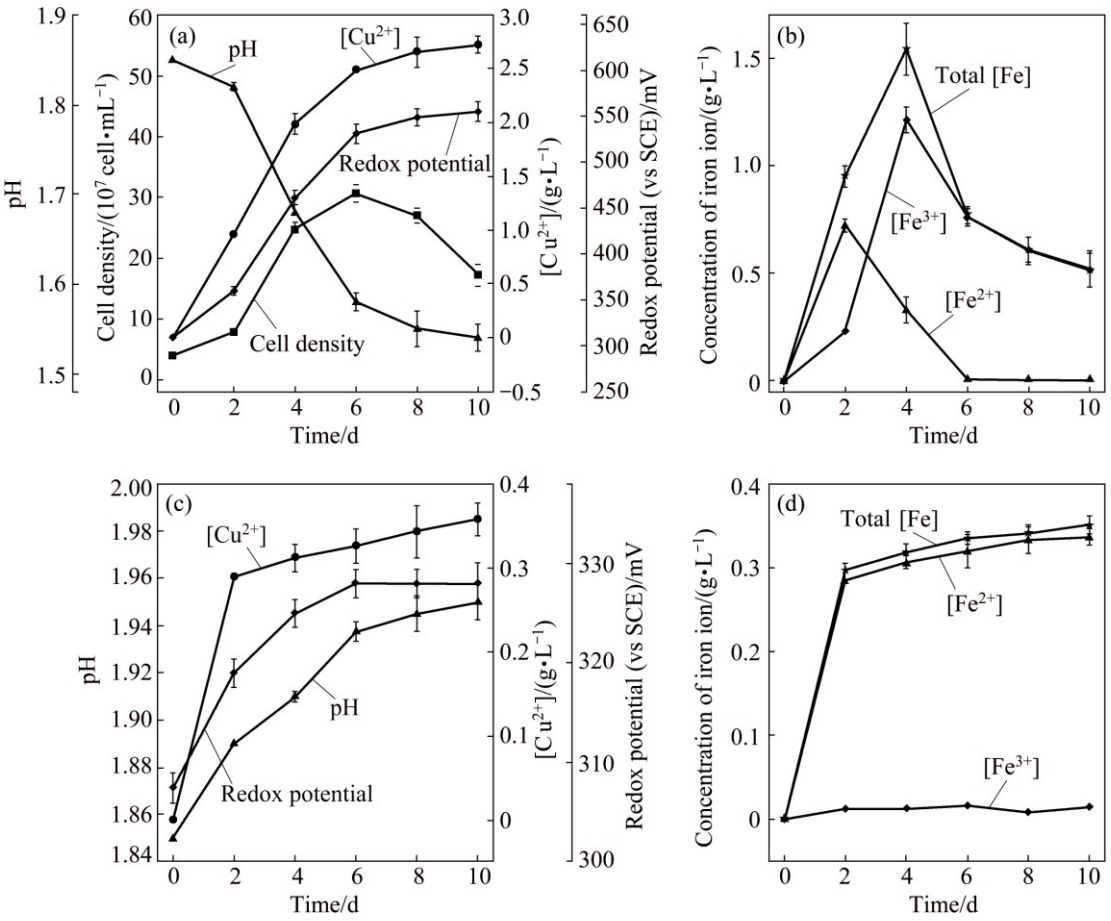


Fig. 1 Leaching behavior of chalcopyrite by *A. manzaensis* (a, b) and in sterile control experiment (c, d)

consuming process (Eq. (2)), which is assured by the slow increasing of pH values in the sterile control experiment (Fig. 1(c)). The rapid decrease in pH values at days 2−6 in bioleaching process may partially result from the oxidation of elemental sulfur (Eq. (3)) [25]. At days 4−6, the concentration of total iron ions declined rapidly (Fig. 1(b)), probably caused by the forming of jarosite (Eq. (5)), which could be accumulated on the surface of chalcopyrite and might be a major factor of hindering copper extraction [2]. It should be noted that jarosite precipitation is an acid-generating reaction (Eq. (5)), so it could also contribute to the pH decline in Fig. 1(a).

$$M^{+}+3Fe^{3+}+2SO_4^{2-}+6H_2O \longrightarrow MFe_3(SO_4)_2(OH)_6+6H^{+} \quad (5)$$

where M is a monovalent cation, such as H_3O^+, K^+, Na^+ or NH_4^+.

3.2 Surface morphology and S, Fe and Cu speciation analyses

The surface morphologies of the chalcopyrite residues during bioleaching and chemical leaching were observed by SEM (Figs. 2(a−f)). SEM results of bioleaching residues showed that the surfaces of chalcopyrite were attacked gradually by *A. manzaensis* and forming structured community on mineral surface (Figs. 2(b−e)). The surface of the original chalcopyrite was smooth. Several bacterial colonies were formed at days 2 and 4, while the leaching products and bacterial colonies were covered over the whole surfaces of the chalcopyrite particles at days 6 and 10. Interestingly, there were some small granules spread visibly on the surface (arrows in Fig. 2). Previous study indicated that it could probably be jarosite [12], which was an important factor in the biofilm formation [26,27]. By contrast, result in Fig. 2(f) showed that little product formed in sterile control experiment and a smooth mineral surface could still be observed after 10 d of leaching.

The results of SR-XRD analysis in Fig. 3(b) showed only little elemental sulfur produced after chemical leaching. However, the SR-XRD patterns of chalcopyrite leached by *A. manzaensis* (Figs. 3(c−f)) became much more complex and the chemical composition changed

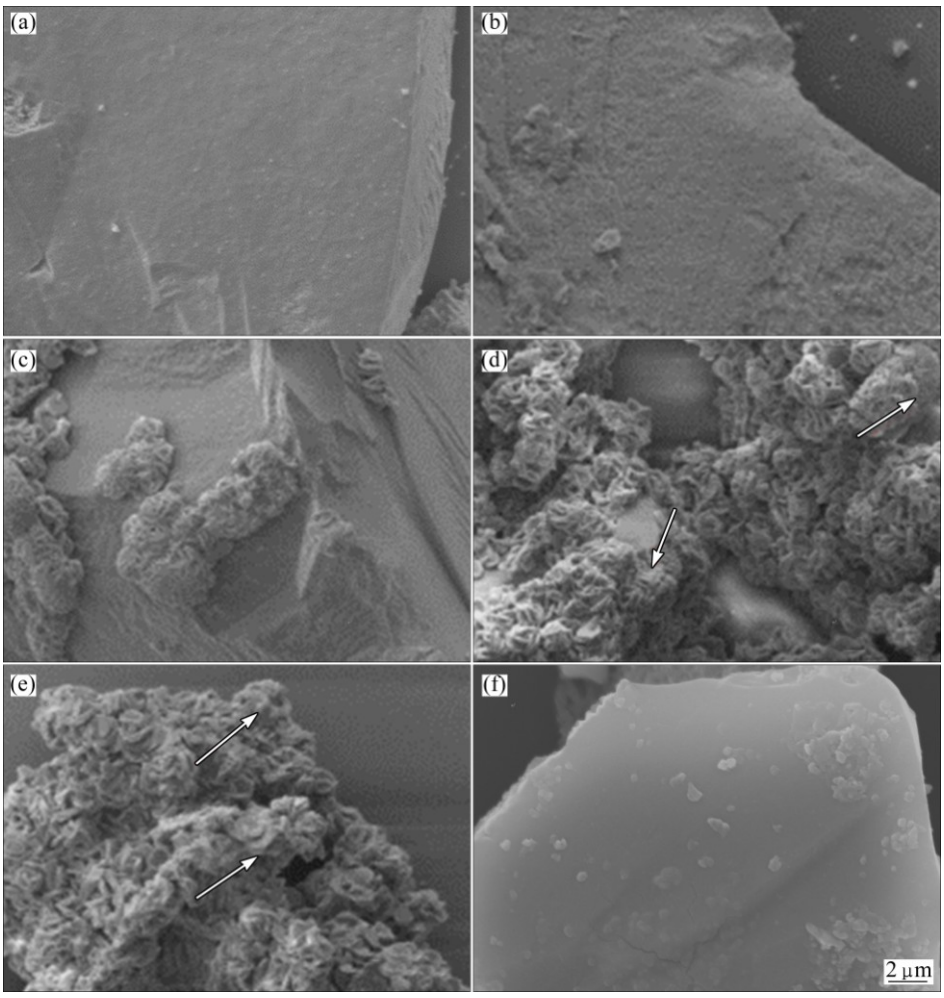


Fig. 2 SEM images of original chalcopyrite (a), and chalcopyrite leached by *A. manzaensis* cells after 2 d (b), 4 d (c), 6 d (d) and 10 d (e), and in sterile control experiment after 10 d (f) (Arrows in Figs. 2(d) and (e) showed that there were some small granules spread visibly on the surface)

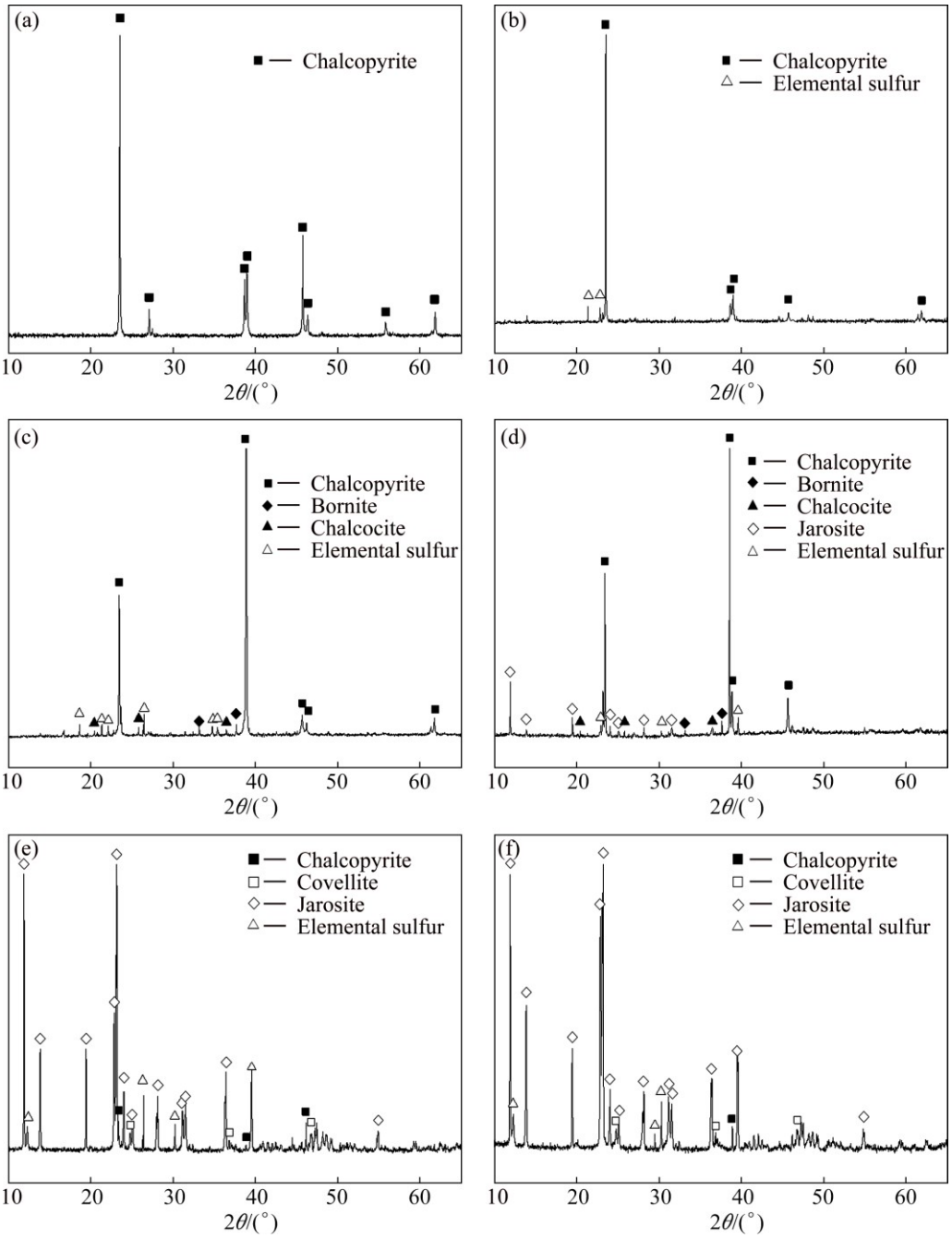


Fig. 3 SR-XRD patterns of original chalcopyrite (a), chalcopyrite leached in sterile control experiment after 10 d (b) and leached by *A. manzaensis* after 2 d (c), 4 d (d), 6 d (e) and 10 d (f)

over time. Results showed that little elemental sulfur, bornite and chalcocite were produced at day 2 (Fig. 3(c)). At day 4, the residue contained jarosite, bornite, chalcocite and elemental sulfur besides chalcopyrite (Fig. 3(d)). At day 6 and day 10, covellite was produced and jarosite gradually became the main component, while the diffraction signals of bornite and chalcocite disappeared (Figs. 3(e−f)).

The S, Fe and Cu K-edge XANES spectra of standard samples (Figs. 4(a), 5(a) and 6(a)) showed clear differences in the peak position and peak intensity and in their absorption edges. Compared with the spectra of standard chalcopyrite, the change of the S, Fe and Cu K-edge XANES spectra of chalcopyrite residues in sterile control experiment (Figs. 4(b), 5(b) and 6(b)) was negligible. However, for the S, Fe and Cu K-edge XANES spectra of chalcopyrite leached by *A. manzaensis* (Figs. 4(b), 5(b) and 6(b)), the intensity of some peaks in the spectra changed gradually. It indicated that, after bioleaching, the S, Fe and Cu speciation of original chalcopyrite was probably gradually transformed into other S, Fe and Cu species.

In order to quantify S, Fe and Cu speciation transformation, the S, Fe and Cu K-edge XANES spectra

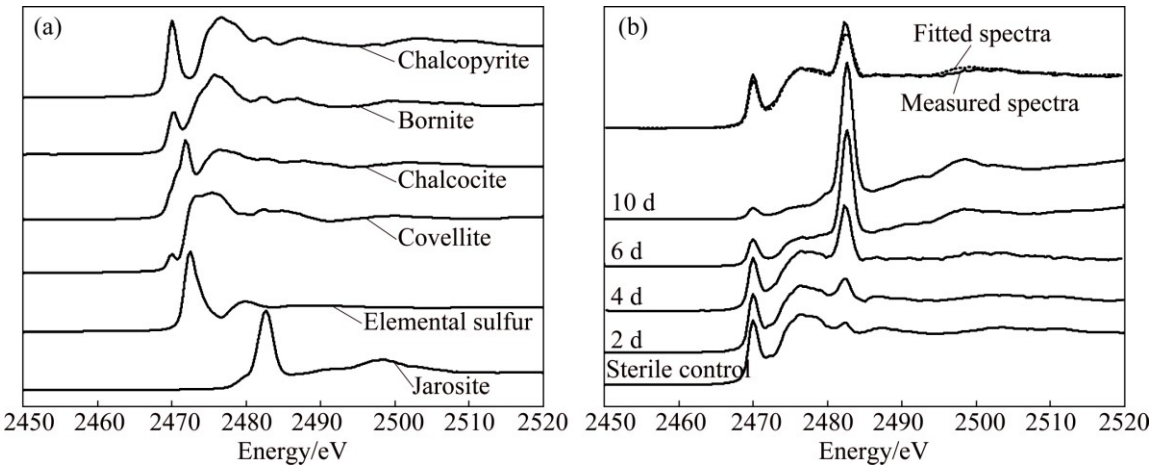


Fig. 4 Normalized S K-edge XANES spectra of standard compounds chalcopyrite, bornite, covellite, chalcocite, jarosite and elemental sulfur (a), and normalized spectra of chalcopyrite leached by *A. manzaensis* at different time (2 d, 4 d, 6 d, 10 d) and in sterile control experiment at day 10 and fitted spectra of bioleaching residue at day 4 (b)

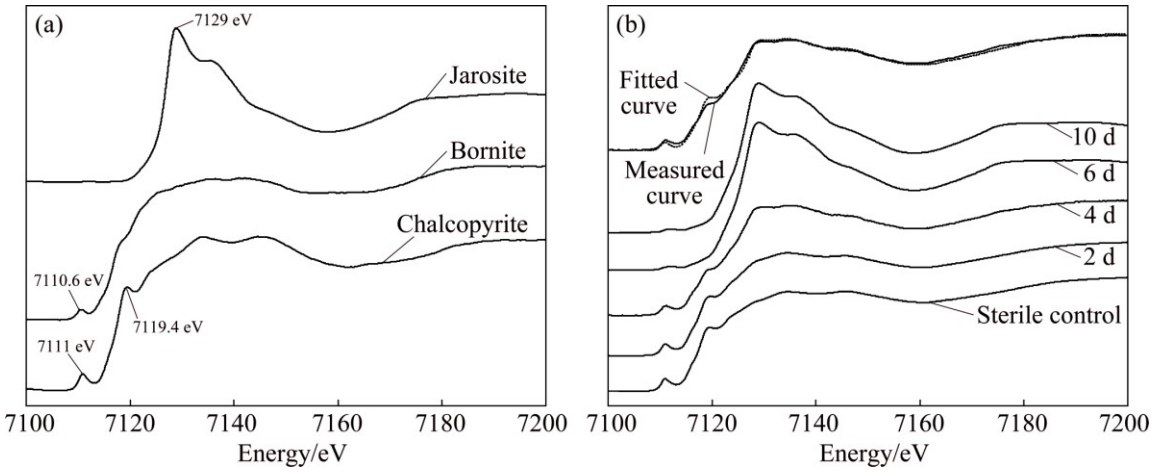


Fig. 5 Normalized Fe K-edge XANES spectra of standard compounds chalcopyrite, bornite, jarosite (a), and normalized spectra of chalcopyrite leached by *A. manzaensis* at different time (2 d, 4 d, 6 d, 10 d) and in sterile control experiment at day 10 and fitted spectra of bioleaching residue at day 4 (b)

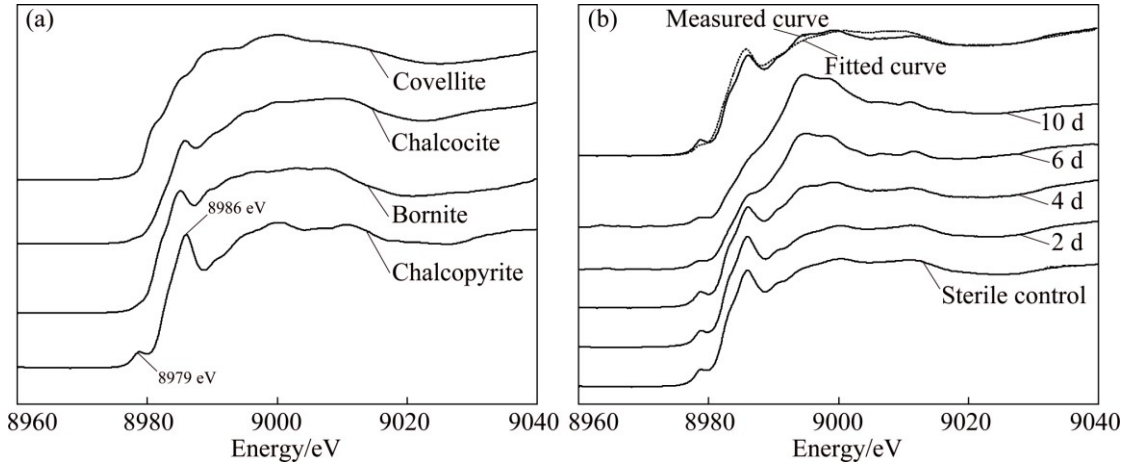


Fig. 6 Normalized Cu K-edge XANES spectra of standard compounds chalcopyrite, bornite, covellite and chalcocite (a), and normalized spectra of chalcopyrite leached by *A. manzaensis* at different time (2 d, 4 d, 6 d, 10 d) and in sterile control experiment at day 10 and fitted spectra of bioleaching residue at day 4 (b)

of these unknown samples (Figs. 4(b), 5(b) and 6(b)) were fitted for their linear composition using the standard spectra of sulfur-compounds (Fig. 4(a)), iron-compounds (Fig. 5(a)) and copper-compounds (Fig. 6(a)), respectively. The fitted results are shown in Tables 1−3, respectively.

Table 1 Fitted results of S K-edge XANES spectra of measured samples (chalcopyrite leached by *A. manzaensis* at different time (2 d, 4 d, 6 d, 10 d) and in sterile control experiment at day 10) with standard spectra of chalcopyrite, bornite, covellite, chalcocite, jarosite and elemental sulfur (S^0)

Sample	Percentage of contribution of standard spectra/%					
	Chalcopyrite	Bornite	Covellite	Chalcocite	Jarosite	S^0
Sterile control	90.1	1.4	−	0.3	2.1	6.1
2 d	81.4	1.9	−	6.1	7.4	5.2
4 d	65.3	2.4	−	8.2	19.7	4.4
6 d	29.7	−	4.8	−	60.6	4.9
10 d	9.2	−	8.3	−	78.8	3.7

Table 2 Fitted results of Fe K-edge XANES spectra of measured samples (chalcopyrite leached by *A. manzaensis* at different time (2 d, 4 d, 6 d, 10 d) and in sterile control experiment at day 10) with standard spectra of chalcopyrite, bornite and jarosite

Sample	Percentage of contribution of standard spectra/%		
	Chalcopyrite	Bornite	Jarosite
Sterile control	95.3	1.8	2.9
2 d	88.3	7.3	4.4
4 d	69.3	4.2	26.5
6 d	34.8	−	65.2
10 d	29.6	−	70.4

Table 3 Fitted results of Cu K-edge XANES spectra of measured samples (chalcopyrite leached by *A. manzaensis* at different time (2 d, 4 d, 6 d, 10 d) and in sterile control experiment at day 10) with standard spectra of chalcopyrite, bornite, covellite and chalcocite

Sample	Percentage of contribution of standard spectra/%			
	Chalcopyrite	Bornite	Chalcocite	Covellite
Sterile control	91.5	4.9	3.6	−
2 d	85.6	6.6	7.8	−
4 d	79.4	10.2	10.4	−
6 d	63.7	−	−	36.3
10 d	58.8	−	−	41.2

The fitted results of S K-edge XANES spectra showed that the sulfur species comprised 81.4% of chalcopyrite, 1.9% of bornite, 6.1% of chalcocite, 7.4% of jarosite and 5.2% of S^0 at day 2, then changed to 65.3% of chalcopyrite, 2.4% of bornite, 8.2% of chalcocite, 19.7% of jarosite and 4.4% of S^0 at day 4; the composition became 29.7% of chalcopyrite, 4.8% of covellite, 60.6% of jarosite and 4.9% of S^0 at day 6, and 9.2% of chalcopyrite, 8.3% of covellite, 78.8% of jarosite and 3.7% of S^0 at day 10 (Table 1). The fitted results of Fe K-edge XANES spectra showed that the iron species comprised 88.3% of chalcopyrite, 7.3% of bornite and 4.4% of jarosite at day 2, then changed to 69.3% of chalcopyrite, 4.2% of bornite and 26.5% of jarosite at day 4; the composition became 34.8% of chalcopyrite and 65.2% of jarosite at day 6, and 29.6% of chalcopyrite and 70.4% of jarosite at day 10 (Table 2). The fitted results of Cu K-edge XANES spectra showed that the copper species comprised 85.6% of chalcopyrite, 6.6% of bornite and 7.8% of chalcocite at day 2, then changed to 79.4% of chalcopyrite, 10.2% of bornite and 10.4% of chalcocite at day 4; the composition became 63.7% of chalcopyrite and 36.3% of covellite at day 6, and 58.8% of chalcopyrite and 41.2% of covellite at day 10 (Table 3). By contrast, only little bornite, chalcocite, jarosite and elemental sulfur were detected for the sterile control experiment.

It should be noted that bornite and chalcocite appeared in the residues at days 2 and 4, and then disappeared from day 6; covellite appeared at day 6 and then increased (Tables 1−3). During bioleaching, jarosite increased with the increase of time and became the main composition gradually (Tables 1 and 2), and elemental sulfur was detected in the whole experiment. These fitted results showed similar trend to SR-XRD results (Fig. 3).

The surface chemistry of chalcopyrite during bioleaching has been studied [2,3,28,29]. According to KLAUBER [2], the dissolution of chalcopyrite could be divided into four stages: 1) an initial reaction of a “fresh” chalcopyrite surface with a high reaction rate and a low redox potential, which is assured in the present study (Fig. 1(a)); 2) thick elemental sulfur layer hinders dissolution; 3) sulfur layer is peeled from the mineral surface; 4) jarosite could be spontaneously formed and precipitated. In the present study, as shown in Fig. 3 and Table 1, elemental sulfur was produced in the initial stage, and the jarosite occurred at day 2 and gradually became the main components at day 10. It can be seen from Fig. 1(a) that with the rapid accumulation of jarosite, copper extraction rate rapidly decreased. Meanwhile, the fitted results of sulfur and iron K-edge XANES spectra showed that, after 10 d of bioleaching, jarosite species accounted for >70% of the leaching residues. It indicated that jarosite might be an important factor hindering the dissolution of chalcopyrite.

According to HARMER et al [3], the observed

elemental sulfur (Fig. 3 and Table 1) was probably formed by a chemical polymerization process from monosulfide (S^{2-}) of bulk chalcopyrite via surface S_n^{2-} species to S_8 (Eq. (6)), which was resulted from the preferential dissolution of metal ions. According to the electrochemical studies by MIKHLIN et al [4] and GHAHREMANINEZHAD et al [5], the release of iron into electrolyte is usually faster than copper, and the iron deficient secondary minerals could be formed. In the present study, the secondary minerals bornite and chalcocite were found in the initial dissolution process. The formation of bornite was considered as a result of the electron transfer in chalcopyrite under oxidizing conditions (Eq. (7)) [7,30]. According to electrochemical behavior of bornite by ARCE and GONZÁLEZ [31], covellite was proposed as oxidation product, as presented by Eqs. (8) and (9).

$$S^{2-} \longrightarrow S_n^{2-} \longrightarrow S_9 \quad (6)$$

$$5CuFeS_2 \longrightarrow Cu_5FeS_4+4Fe^{3+}+6S^0+12e \quad (7)$$

$$Cu_5FeS_4 \longrightarrow Cu_{5-x}FeS_4+xCu^{2+}+2xe \quad (8)$$

$$Cu_{5-x}FeS_4+6H^+ \longrightarrow CuS+(4-x)Cu^{2+}+3H_2S+Fe^{3+}+(5-x)e \quad (9)$$

In a two-step dissolution model proposed by HIROYOSHI et al [32], the dissolution of chalcopyrite was speculated to be reduced firstly by Fe^{2+} to chalcocite (Cu_2S) at low potential (Eq. (10)). This study showed that chalcocite observed at days 2 and 4 (Figs. 3(c) and (d)) and the composition of chalcocite on the surface of chalcopyrite is 7.8% and 10.4%, respectively (Table 3), where the redox potential value was about 360 mV and 461 mV, respectively (Fig. 1(a)). Previous studies also showed that covellite could be converted by chalcocite in the bioleaching of chalcopyrite by thermophiles, as presented by (Eq. (11)) [10,21,23], which was assured by the observed covellite in this study at days 6 and 10.

$$CuFeS_2+3Cu^{2+}+3Fe^{2+} \longrightarrow 2Cu_2S+4Fe^{3+} \quad (10)$$

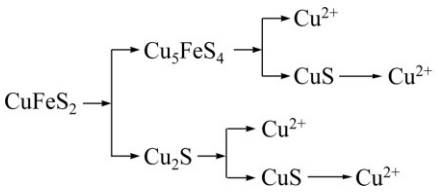
$$Cu_2S+2Fe^{3+} \longrightarrow Cu^{2+}+2Fe^{2+}+CuS \quad (11)$$

3.3 Formation and evolution of second minerals during bioleaching based SR-XRD and XANES spectroscopy

By combining SR-XRD and XANES spectroscopy, this study also presents a new method to analyze the surface chemical species qualitatively and quantitatively. In the previous description merely based on S K-edge XANES analysis [12], only covellite was identified as transient intermediate compound, while other secondary minerals cannot be assured. In addition, the quantitative analysis of unknown XANES spectra is always done by linear combination fitting with the assistance of standards [20,33]. Though the quantitative analysis method has been widely accepted used, the calculation of the unknown spectra may be not always reliable when the spectra of standard samples are not fully or properly selected [33−35]. The combining SR-XRD and XANES spectroscopy could well solve this shortage. The composition is first qualitatively analyzed by SR-XRD, and then the mineral surface is quantitatively analyzed to make sure the content of each composition by XANES spectroscopy. On the other hand, since some peaks of the XANES spectra of the standard minerals are so similar, they may also affect the identity of the composition of the unknown spectra (Figs. 4(a), 5(a) and 6(a)). However, though there may exist some errors when these unknown spectra are linearly fitted by using the standard spectra, the comprehensive analyses based on the SR-XRD analysis and the XANES spectroscopy of all of the three elements (i.e., S, Fe and Cu) will provide more convincing results. And these results could verify each other.

In the present study, the redox potential value curve (Fig. 1(a)) during bioleaching of chalcopyrite by *A. manzaensis* showed that the redox potential value was increased with the increase of time at days 2 and 4, and then tended to slow when reached 531−550 mV. Furthermore, S, Fe and Cu speciation also showed that bornite and chalcocite presented in the bioleaching residues at days 2 and 4, thereafter disappeared, and then covellite appeared at day 6 and then increased (Tables 1−3). Jarosite and elemental sulfur were also formed in the bioleaching process (Fig. 3, Tables 1 and 2) and jarosite was gradually increased with increase of time, and became the major component at the end of bioleaching. Therefore, this study indicated that metal-deficiency sulfides chalcocite and bornite could be first formed at the initiation of bioleaching at a low redox potential value (360−461 mV), and then gradually transformed to covellite with a high redox potential value (461−531 mV).

By using the SR-XRD and XANES spectroscopy, we confirmed that metal deficiency metal sulfide can be formed and further quantified the composition on the surface of chalcopyrite during bioleaching of chalcopyrite by *A. manzaensis*. Based on the above discussion, we can speculate that the dissolution of chalcopyrite is as follows (Eq. (12)).



(12)

4 Conclusions

1) Bioleaching experiment of chalcopyrite showed that the copper concentration was 2.72 g/L after 10 d of

bioleaching by *A. manzaensis*, corresponding to 82.4% copper extraction, indicating that this thermoacidophilic Archaea strain could significantly promote copper extraction.

2) SEM results showed that the surfaces of chalcopyrite were corroded gradually by *A. manzaensis*.

3) By combining SR-XRD and XANES, a method for qualitative and quantitative analyses of the surface chemical composition of the minerals was provided. Results indicated that chalcocite and bornite could be firstly formed at the initiation of bioleaching with a low redox potential value, and then gradually transformed to covellite with a high redox potential value. Meanwhile, elemental sulfur and jarosite were also confirmed as the important products during the dissolution of chalcopyrite by *A. manzaensis*.

References

[1] PRADHAN N, NATHSARMA K C, SRINIVASA RAO K, SUKLA L B, MISHRA B K. Heap bioleaching of chalcopyrite: A review [J]. Minerals Engineering, 2008, 21(5): 355−365.

[2] KLAUBER C. A critical review of the surface chemistry of acidic ferric sulphate dissolution of chalcopyrite with regards to hindered dissolution [J]. International Journal of Mineral Processing, 2008, 86(1−4): 1−17.

[3] HARMER S L, THOMAS J E, FORNASIERO D, GERSON A R. The evolution of surface layers formed during chalcopyrite leaching [J]. Geochimica et Cosmochimica Acta, 2006, 70(17): 4392−4402.

[4] MIKHLIN Y L, TOMASHEVICH Y V, ASANOV I P, OKOTRUB A V, VARNEK V A, VYALIKH D V. Spectroscopic and electrochemical characterization of the surface layers of chalcopyrite ($CuFeS_2$) reacted in acidic solutions [J]. Applied Surface Science, 2004, 225(1−4): 395−409.

[5] GHAHREMANINEZHAD A, ASSELIN E, DIXON D G. Electrochemical evaluation of the surface of chalcopyrite during dissolution in sulfuric acid solution [J]. Electrochimica Acta, 2010, 55(18): 5041−5056.

[6] YANG Y, LIU W, CHEN M. A copper and iron K-edge XANES study on chalcopyrite leached by mesophiles and moderate thermophiles [J]. Minerals Engineering, 2013, 48: 31−35.

[7] MAJUSTE D, CIMINELLI V S T, OSSEO-ASARE K, DANTAS M S S, MAGALHÃES-PANIAGO R. Electrochemical dissolution of chalcopyrite: Detection of bornite by synchrotron small angle X-ray diffraction and its correlation with the hindered dissolution process [J]. Hydrometallurgy, 2012, 111−112: 114−123.

[8] FERRER S, PETROFF Y. Surface science done at third generation synchrotron radiation facilities [J]. Surface Science, 2002, 500(1−3): 605−627.

[9] LOBINSKI R, MOULIN C, ORTEGA R. Imaging and speciation of trace elements in biological environment [J]. Biochimie, 2006, 88(11): 1591−1604.

[10] ZHU W, XIA J L, YANG Y, NIE Z Y, ZHENG L, MA C Y, ZHANG R Y, PENG A A, TANG L, QIU G Z. Sulfur oxidation activities of pure and mixed thermophiles and sulfur speciation in bioleaching of chalcopyrite [J]. BioresourceTechnology, 2011, 102(4): 3877−3882.

[11] XIA J L, YANG Y, HE H, ZHAO X J, LIANG C L, ZHENG L, MA C Y, ZHAO Y D, NIE Z Y, QIU G Z. Surface analysis of sulfur speciation on pyrite bioleached by extreme thermophile *Acidianus manzaensis* using Raman and XANES spectroscopy [J]. Hydrometallurgy, 2010, 100(3−4): 129−135.

[12] HE H, XIA J L, YANG Y, JIANG H, XIAO C Q, ZHENG L, MA C Y, ZHAO Y D, QIU G Z. Sulfur speciation on the surface of chalcopyrite leached by *Acidianus manzaensis* [J]. Hydrometallurgy, 2009, 99(1−2): 45−50.

[13] SALVADO N, BUTI S, NICHOLSON J, EMERICH H, LABRADOR A, PRADELL T. Identification of reaction compounds in micrometric layers from gothic paintings using combined SR-XRD and SR-FTIR [J]. Talanta, 2009, 79(2): 419−428.

[14] DU PLESSIS C, BATTY J, DEW D. Commercial applications of thermophile bioleaching [C]//RAWLINGS D E, JOHNSON D B. Heidelberg: Springer, 2007: 57−80.

[15] LIANG C L, XIA J L, NIE Z Y, YANG Y, MA C Y. Effect of sodium chloride on sulfur speciation of chalcopyrite bioleached by the extreme thermophile *Acidianus manzaensis* [J]. Bioresource Technology, 2012, 110: 462−467.

[16] LIU H C, NIE Z Y, XIA J L, ZHU H R, YANG Y, ZHAO C H, ZHENG L, ZHAO Y D. Investigation of copper, iron and sulfur speciation during bioleaching of chalcopyrite by moderate thermophile *Sulfobacillus thermosulfidooxidans* [J]. International Journal of Mineral Processing, 2015, 137: 1−8.

[17] LIU H C, XIA J L, NIE Z Y. Relatedness of Cu and Fe speciation to chalcopyrite bioleaching by *Acidithiobacillus ferrooxidans* [J]. Hydrometallurgy, 2015, 156: 40−46.

[18] LIU Hong-chang, XIA Jin-lan, NIE Zhen-yuan, MA Ya-long, MA Chen-yan, ZHENG Lei, HONG Cai-hao, ZHAO Yi-dong. Iron L-edge and L-edge XANES spectroscopy analysis of pyrite leached by *Acidianus manzaensis* [J]. Transactions Nonferrous Metals Society of China, 2015, 25(7): 2407−2414.

[19] LIU Hong-chang, XIA Jin-lan, NIE Zhen-yuan, ZHENG Lei, MA Chen-yan, ZHAO Yi-dong. Differential utilization and speciation transformation of orthorhombic α-S_8 and amorphous μ-S by substrate-acclimated mesophilic *Acidithiobacillus ferrooxidans* [J]. Transactions of Nonferrous Metals Society of China, 2015, 25(9): 3096−3102.

[20] RAVEL B, NEWVILLE M, ATHENA, ARTEMIS, HEPHAESTUS: Data analysis for X-ray absorption spectroscopy using IFEFFIT [J]. Journal of Synchrotron Radiation, 2005, 12(4): 537−541.

[21] LIANG C L, XIA J L, ZHAO X J, YANG Y, GONG S Q, NIE Z Y, MA C Y, ZHENG L, ZHAO Y D, QIU G Z. Effect of activated carbon on chalcopyrite bioleaching with extreme thermophile *Acidianus manzaensis* [J]. Hydrometallurgy, 2010, 105(1−2): 179−185.

[22] GERICKE M, PINCHES A, van ROOYEN J V. Bioleaching of a chalcopyrite concentrate using an extremely thermophilic culture [J]. International Journal of Mineral Processing, 2000, 62(1−4): 243−255.

[23] WATLING H R. The bioleaching of sulphide minerals with emphasis on copper sulphides—A review [J]. Hydrometallurgy, 2006, 84(1−2): 81−108.

[24] ROHWERDER T, GEHRKE T, KINZLER K, SAND W. Bioleaching review part A: Progress in bioleaching: fundamentals and mechanisms of bacterial metal sulfide oxidation [J]. Applied Microbiology and Biotechnology, 2003, 63(3): 239−248.

[25] VILCÁEZ J, SUTO K, INOUE C. Response of thermophiles to the simultaneous addition of sulfur and ferric ion to enhance the bioleaching of chalcopyrite [J]. Minerals Engineering, 2008, 21(15): 1063−1074.

[26] KARAMANEV D G. Model of the biofilm structure of *Thiobacillus ferrooxidans* [J]. Journal of Biotechnology, 1991, 20(1): 51−64.

[27] POGLIANI C, DONATI E. Immobilisation of *Thiobacillus ferrooxidans*: Importance of jarosite precipitation [J]. Process Biochemistry, 2000, 35(9): 997−1004.

[28] RODRíGUEZ Y, BALLESTER A, BLÁZQUEZ M L, GONZÁLEZ

F, MUÑOZ J A. New information on the chalcopyrite bioleaching mechanism at low and high temperature [J]. Hydrometallurgy, 2003, 71(1−2): 47−56.

[29] DEVASIA P, NATARAJAN K A, SATHYANARAYANA D N, RAMANANDA G, RAO G R. Surface chemistry of *Thiobacillus ferrooxidans* relevant to adhesion on mineral surfaces [J]. Applied and Environmental Microbiology, 1993, 59(12): 4051−4055.

[30] ACERO P, CAMA J, AYORA C. Kinetics of chalcopyrite dissolution at pH 3 [J]. European Journal of Mineralogy, 2007, 19(2): 173−182.

[31] ARCE E M, GONZÁLEZ I. A comparative study of electrochemical behavior of chalcopyrite, chalcocite and bornite in sulfuric acid solution [J]. International Journal of Mineral Processing, 2002, 67(1−4): 17−28.

[32] HIROYOSHI N, ARAI M, MIKI H, TSUNEKAWA M, HIRAJIMA T. A new reaction model for the catalytic effect of silver ions on chalcopyrite leaching in sulfuric acid solutions [J]. Hydrometallurgy, 2002, 63(3): 257−267.

[33] DAHL C, FRIEDRICH C G. Microbial sulfur metabolism [M]. Heidelberg: Springer, 2008.

[34] REHR J J, ANKUDINOV A L. Progress in the theory and interpretation of XANES [J]. Coordination Chemistry Reviews, 2005, 249(1−2): 131−140.

[35] REHR J J, ANKUDINOV A L. Progress and challenges in the theory and interpretation of X-ray spectra [J]. Journal of Synchrotron Radiation, 2001, 8(2): 61−65.

嗜酸热古菌 *Acidianus manzaensis* 浸出黄铜矿过程中次生矿物的形成及演变

刘红昌[1,2]，夏金兰[1,2]，聂珍媛[1,2]，文 闻[3]，杨 云[1,2]，马陈燕[4]，郑 雷[4]，赵屹东[4]

1. 中南大学 资源加工与生物工程学院，长沙 410083；
2. 中南大学 生物冶金教育部重点实验室，长沙 410083；
3. 中国科学院 上海应用物理研究所 上海光源，上海 201204；
4. 中国科学院 高能物理研究所 北京同步辐射装置，北京 100049

摘 要：基于同步辐射 X 射线衍射(SR-XRD)和硫/铁/铜 K 边 X 射线吸收近边结构(XANES)光谱学等技术，研究了嗜酸热古菌 *Acidianus manzaensis* 浸出黄铜矿过程中次级产物的形成和演变机制。浸出实验结果表明，经过 10 d 的生物浸出黄铜矿的浸出率为 82.4%，此时黄铜矿的表面被显著腐蚀且覆盖了一层浸出产物。在生物浸出过程中，矿物表面次级产物的形成及演变有如下规律：1)第 2 d 和第 4 d 检测了少量单质硫、斑铜矿和辉铜矿；2)第 6 d 和 10 d 斑铜矿和辉铜矿消失，但是铜蓝开始产生，并且黄钾铁矾逐渐变成主要产物。这些结果表明浸出过程中首先在低电位(360~461 mV)下形成金属缺失型辉铜矿和斑铜矿，随着电位升高，在高电位(461~531 mV)下逐渐转化为了铜蓝。

关键词：生物冶金；黄铜矿；*Acidianus manzaensis*；次生矿物；形成；演变

(Edited by Yun-bin HE)